Inverted to Normal Phase Transition in Solution-Cast Polystyrene−Poly(methyl methacrylate) Block Copolymer Thin Films

Yumei Gong, Haiying Huang, Zhijun Hu, Yongzhong Chen, Dongju Chen, Zongbao Wang, and Tianbai He*

State Key Laboratory of Polymer Physics and Chemistry, Changchun Institute of Applied Chemistry, Chinese Academy of Sciences, Changchun, 130022, P. R. China

Received November 8, 2005; Revised Manuscript Received March 7, 2006

ABSTRACT: We have investigated the inverted phase formation and the transition from inverted to normal phase for a cylinder-forming polystyrene-*block*-poly(methyl methacrylate) (PS-*b*-PMMA) diblock copolymer in solution-cast films with thickness about 300 nm during the process of the solution concentrating by slow solvent evaporation. The cast solvent is 1,1,2,2-tetrachloroethane (Tetra-CE), a good solvent for both blocks but having preferential affinity for the minority PMMA block. During such solution concentrating process, the phase behavior was examined by freeze-drying the samples at different evaporation time, corresponding to at different block copolymer concentrations, φ. As φ increases from ~0.1% (v/v), the phase structure evolved from the disordered sphere phase (DS), consisting of random arranged spheres with the majority PS block as a core and the minority PMMA block as a corona, to ordered inverted phases including inverted spheres (IS), inverted cylinders (IC), and inverted hexagonally perforated lamellae (IHPL) with the minority PMMA block comprising the continuum phase, and then to the lamellar (LAM) phase with alternate layers of the two blocks, and finally to the normal cylinder (NC) phase with the majority PS block comprising the continuum phase. The solvent nature and the copolymer solution concentration are shown to be mainly responsible for the inverted phase formation and the phase transition process.

The phase behavior of block copolymer thin films has been studied for many years and continues to be an active area of research in both experimental and theoretical points of view.[1−26] It has been well established that block copolymers can self-assemble into spheres, cylinders, lamellae, or bicontinuous double diamonds, depending on the volume fraction of the components, *f*. Moreover, with the same material, different morphologies can be observed in response to the film preparation conditions, such as the application of external fields,[3−16] type of solvent used,[5−16] amount of solvent uptake,[8,15−19] solvent evaporation rate,[7,13−15,19] and film confinement conditions.[14,16,25,26]

The preparation of block copolymer thin films under various solvent evaporation conditions turns out to be an effective and direct method to control the microdomain structures.[7−17] During such a sample preparation process, the nature of the solvent is one of the key factors that determine the resultant microstructures. By annealing the block copolymer thin films in the vapor of different solvents, one can access different morphologies.[8,9] Moreover, by using different casting solvents, various metastable morphologies deviated from the thermodynamically equilibrium morphology can be achieved in block copolymer thin films.[10−17] Among them, the inverted phase (the minority blocks comprising the continuum phase) uncovered by our group in cylinder-forming poly(styrene−butadiene−styrene) (SBS)[13−15] and poly(styrene−butadiene) (SB)[13,14] block copolymers is an intriguing finding since the observation evidently differs from numerous of publications dealing with cylinder-forming block copolymer thin films. Moreover, with the copolymer concentration increasing, the inverted phase can transform back to the normal phase (the majority blocks comprising the continuum phase).[13] However, in the experiment, the two components of the block copolymers used have large differences in the viscoelasticity (bulk moduli of polystyrene (PS) and polybutadiene (PB) are ~ 5.0 and ~ 1.9 GPa, respectively[27]) and large differences in the glass transition temperatures (T_g of PS and PB are ~100 and ~−80 °C, respectively[27]), this characteristic makes the effect of solvent on the formation of inverted phase more complicated. As simulated by Yang et al.,[28] the viscoelastic effect of a block in diblock copolymers is expected to be largely responsible for the observed deviations from normal phase separation. On the other hand, based on the mean field theory, one can speculate that there must be a multiple transition from inverted to normal phase, i.e., from A-rich microdomains dispersed in a B-rich matrix to B-rich microdomains dispersed in an A-rich matrix, involving the interfacial curvature alteration.[1] Therefore, an in-depth understanding of the inverted phase formation as well as the transition to normal phase with the copolymer concentration increasing continues to be a fascinating and stimulating area.

In the present paper, we extend our investigation to another block copolymer to explore the mechanism of inverted phase formation and the transition process from inverted to normal phase. To avoid a large difference in characteristics between the two blocks, a different kind of material, the PS-*b*-PMMA block copolymer, was selected in this work, where both PS and poly(methyl methacrylate) (PMMA) blocks have comparable glass transition temperatures (T_g of PS and PMMA are ~100 and ~105 °C, respectively[27]) and bulk modulus (bulk moduli of PS and PMMA are ~5.0 and ~5.1 GPa, respectively[27]). We convinced that the similar phase behavior observed in rather different kinds of materials can reveal information on the general concept of nature. The solvent chosen for the current study is 1,1,2,2-tetrachloroethane (Tetra-CE), a good solvent for both blocks, but which has a preferential affinity for the PMMA block. The advantage of the solvent is that it has a higher boiling temperature and a lower vapor pressure (T_b ~ 146 °C; vapor pressure ~ 6.1 mmHg at 25 °C[29]), which make the solvent evaporation quite slow. That is, it allows us to investigate in

* To whom correspondence should be addressed. E-mail: tbhe@ciac.jl.cn.

10.1021/ma052380k CCC: $33.50
Published on Web 04/08/2006

Table 1. Phase Structure Features of the Solution-Cast Film as a Function of Copolymer Concentration[a]

copolymer concentration φ (% v/v)	0.1	1	10	13	16	30	40	43	55	≳82
phase structure	DS	DS	IS	IS & IC	IC	UIC	IHPL	LAM	LAM	NC

[a] Key: DS = disordered spheres; IS = inverted spheres; IC = inverted cylinders; UIC = undulated inverted cylinders; IHPL = inverted hexagonally perforated lamellae; LAM = lamellae; NC = normal cylinders.

more detail of the phase sequence from inverted to normal with the copolymer concentration increasing. Under an extremely slow solvent evaporation rate (to eliminate the morphologies controlled by kinetics of solvent evaporation and meanwhile to obtain the equilibrium normal phase after complete solvent evaporation[16]), we apply the freeze-drying method to detect the details of the phase behavior. During the solvent evaporation, the concentration of polymer solution gradually increases, as it must experience a process from dilute solution to concentrated solution before formation of a solid thin film. In this way, the morphologies frozen at different times correspond to kinetically freezing-in phase structures at different block copolymer concentrations, φ; i.e., the morphology observed in the solution-cast films can be considered to be the memory of the domain structure which existed in the solution.[13]

Experimental Section

Materials. The block copolymer used in this paper, PS_{1257}-*b*-$PMMA_{460}$ (the numbers in subscript refer to the number-average degree of polymerization of each block), with polydispersity index 1.10 was purchased from Polymer Source Inc. and used as received. In the bulk, the copolymer is expected to adopt a hexagonal microstructure with PMMA cylinders embedded in a PS matrix.[1] A solvent 1,1,2,2-tetrachloroethane (Tetra-CE) was employed to dissolve the copolymer. The relative affinity of the solvent for each block can be estimated from the polymer−solvent interaction parameters, $\chi_{PS\text{-}Tetra\text{-}CE} = 0.435 < 0.5$ and $\chi_{PMMA\text{-}Tetra\text{-}CE} = 0.374 < 0.5$ at room temperature (∼ 25 °C). That is, Tetra-CE is good for both blocks but has a preferential affinity for the minority PMMA block. (That Tetra-CE is a good solvent for PS has been confirmed by Cantor et al.[30]) The expression $\chi_{P\text{-}S} = 0.34 + V_S(\delta_S - \delta_P)^2/RT$[27] is used in calculating the polymer−solvent interaction parameters, where V_S is the molar volume of the solvent (104.9 cm^3/mol for Tetra-CE), R is the gas constant, T is the temperature, and δ_S and δ_P are the solubility parameters of solvent and polymer. In the present system, the solubility parameters of solvent and polymers are $\delta_S = 20.1$ $(J/cm^3)^{1/2}$, $\delta_{PS} = 18.6$ $(J/cm^3)^{1/2}$, and $\delta_{PMMA} = 19.2$ $(J/cm^3)^{1/2}$, respectively.[27,29]

Sample Preparation. In the experiment, the copolymer was dissolved in Tetra-CE to produce a solution with initial copolymer concentration $\varphi \sim 0.1\%$ (v/v). Such low initial concentration enables us to conveniently follow the concentration increasing process by the solvent evaporation and correspondingly to follow the phase structure evolution process. For freeze-drying experiment, a 40 μL pipet was used to cast equal-sized droplets of the solution onto carbon-coated mica. After complete solvent evaporation, it results in a film with thickness of ca. 300 nm, which is much thicker than the boundary effects extending distance about one microdomain spacing, ∼67 nm for the present block copolymer.[16] An extremely slow solvent evaporation condition was adopted, which was achieved by allowing the solution-cast films to be exposed in a Tetra-CE vapor atmosphere (a few drops of Tetra-CE were precast around the substrate) in a small dish completely covered with a lid. The longest time when the as-cast solution was completely dried at room temperature is approximately 20 days. During the solution-to-film process, we select different evaporation times to freeze-in the transient phase structures of solution-cast films, which corresponds to kinetically locking the phase structures at different solution concentrations, φ. This procedure was performed by using liquid nitrogen to quench the small dish when time is reached, so that the samples were frozen-in in a few seconds. Finally, the frozen samples were transferred to another airtight chamber connected with a pump; and the frozen solvent was then sublimed in a vacuum (10^{-4} Torr) for 2 days to obtain a solid-state sample. To keep the samples in the frozen state, the airtight chamber will be immersed in liquid nitrogen in the whole freeze-drying process.

At the same time, to measure the copolymer concentration in the solution-cast film at different evaporation times, reproducible experiments were performed at the given times. The concentration φ was calculated by weighing the loss of the films and given by $\varphi = ((W_P/\rho_P)/((W - W_P)/\rho_S + W_P/\rho_P)) \times 100\%$, assuming additivity of volumes, where W_P is the weight of block copolymer in the cast solution calculated from the initial solution concentration and the volume of cast solution, W is the weight of the cast solution measured at different evaporation time, and ρ_P and ρ_S are the densities of the block copolymer and the solvent, respectively. ($\rho_P \sim 1.08$ g/cm^3 assuming additivity of volumes of PS and PMMA, $\rho_{PS} = 1.05$ g/cm^3, $\rho_{PMMA} = 1.17$ g/cm^3, and $\rho_S = 1.6$ g/cm^3.)[27,29] A curve of the average calculated concentration of several reproduced experiments as a function of solvent evaporation time was plotted, as shown in Supporting Information in Figure S1. The polymer concentration at different evaporation time can be obtained conveniently from the curve.

Instruments. The tapping mode atomic force microscopy (AFM) measurement was carried out on a commercial SPA-300HV/SPI3800 N with an SPI 3800 N controller (Seiko Instruments Inc., Japan). The AFM cantilever (spring constant 2 N/m, Olympus Co. Japan) was driven to oscillate at ∼ 70 kHz, close to the cantilever's resonant frequency. More than five regions (include edge and center) of each film were examined and no significant changes of the morphologies is observed even though there is some thickness variation in the films.

Transmission electron microscopy (TEM) experiments were conducted on a JEOL 2010 electron microscope, operating at 200 kV accelerating voltage in a bright-field mode. For plain-view TEM microscopy, the films were floated off from carbon-coated micas in distilled water and collected onto copper TEM grids. For cross-sectional TEM microscopy, some portions of the floated film were collected on a piece of epoxy and dried. After staining with RuO_4 and vacuum evaporated a layer of carbon on the copolymer film, the epoxy piece together with the copolymer film were embedded in epoxy and subsequently cured at 35, 45, and 55 °C for respective 12 h. The carbon coating can simultaneously prevent swelling of the copolymer film by the uncured epoxy and enhance adhesion at the epoxy-copolymer interface. The ultrathin sections with ca. 70 nm thickness were microtomed using a LEICA Ultracut R microtome and a glass knife at −50 °C and were collected onto carbon-coated copper TEM grids. All TEM samples were then stained by exposure in RuO_4 vapor to selectively stain the PS block, so in all the TEM micrographs presented here the PS phase appears dark and the PMMA phase appears bright.

Results

As is known, the control with different solvent evaporation times leads to frozen-in microstructures corresponding to different block copolymer solution concentrations, φ.[13] On the basis of the relationship between the calculated copolymer concentration of the sample and the evaporation time (Figure S1), we will describe the film morphologies in a sequence where the copolymer concentration is increasing. The phase structure features of the films are summarized in Table 1. As is shown, with the copolymer concentration increasing, complex phase behavior including disordered sphere and various inverted and normal phases was observed. The results can be divided into

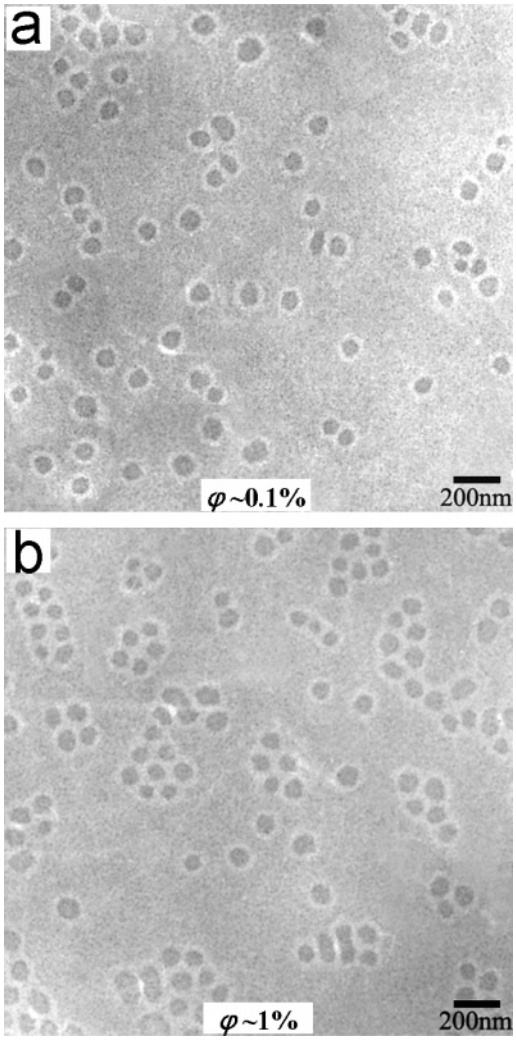

Figure 1. (a,b) Bright-field TEM micrographs of the solution-cast film freeze-dried at different copolymer concentrations as indicated, which show the disordered sphere phase. Before imaging, the samples were selectively stained by RuO_4. Therefore, the dark regions are PS and the bright regions are PMMA.

four parts according to the microstructure characteristics: the disordered sphere phase structure in Figure 1, the inverted phase structures in Figure 2, the lamellar phase structure in Figure 3, and the normal phase structure in Figure 4.

Figure 1a displays the TEM micrograph of the solution-cast film freeze-dried at the initial concentration $\varphi \sim 0.1\%$ (v/v). At this concentration, the film is characterized by random arranged dark circular objects. Since the phase structure of a film obtained by freeze-drying can be considered to represent the memory of the phase structure that existed in solution,[13] the geometry of the objects should be spherical in low concentration solutions to make the interfacial energy the lowest.[31] The circular objects in Figure 1a obtained in the solution-cast film freeze-dried at such a low copolymer concentration may best be described as spheres. Moreover, they are micelle-like spheres comprising a core formed by RuO_4 selectively stained PS surrounded by a PMMA corona. It can be deduced from the polymer−solvent interaction parameters ($\chi_{PS\text{-}Tetra\text{-}CE} = 0.435$ and $\chi_{PMMA\text{-}Tetra\text{-}CE} = 0.374$) that the solvent Tetra-CE has a preferential affinity for the minority PMMA block, which induces the less soluble majority PS block to take a compact conformation and form a central core and the PMMA to be somewhat pushed toward the outside as a result of the repulsive interactions between PS and PMMA blocks.[16,31] The diameter of the spheres determined from the TEM micrograph in Figure 1a is 85 ± 5 nm.

Comparing the volumes occupied by PS and PMMA in the TEM micrograph in Figure 1a, PS evidently occupies more space than PMMA, which is consistent with the composition of the bulk copolymer that PS is the majority block, even though the film clearly develops a structure which can only be formed for a PS included phase due to the preferential affinity of solvent for the minority PMMA block as depicted above. Nevertheless, one may argue that the fact that the PMMA occupies less space is related to the PMMA probable degradation in the electron beam. In fact, there are few works[25] known to observe the probable PMMA degradation in the electron beam during TEM measurements. Meanwhile, whether such degradation of PMMA block occurs or not, there was no report of a change in phase structure resulting from the degradation of PMMA. Therefore, we deem that the phase structure measured by TEM is the actual structure of the sample.

The disordered sphere phase persists with the number of spheres increasing as the copolymer concentration increases. Figure 1b shows the TEM micrograph of the film obtained at $\varphi \sim 1\%$ (v/v). Obviously, the spheres have been locally close-packed.

The number of spheres continues increasing until the concentration of the copolymer attains $\varphi \sim 10\%$ (v/v), at which a compact morphology was observed. The in-plane and cross-sectional TEM micrographs of such a morphology are shown in Figure 2a. The in-plane view of the film (Figure 2a) shows a morphology of dark spherical PS microdomains with average diameter of 85 nm packed hexagonally dispersing in a matrix of bright PMMA. The cross-sectional view of the film (the inset in Figure 2a) also reveals that PS forms spherical microdomains with diameter of 85 ± 7 nm, which are embedded in a PMMA matrix. The bright layers at both top and bottom interfaces between the epoxy embedding medium and the film in such a cross-sectional micrograph are the electron beam transmitted carbon coatings. The cross-sectional micrograph also shows that the total film thickness is ca. 350−380 nm and that the structures between the surface and the interior of the film are uniform. Therefore, the phase structure as shown in Figure 2a obtained at $\varphi \sim 10\%$ (v/v) should be inverted spheres in which the minority PMMA block forms the continuum phase.[13−15]

With further concentration of the solution, the PS spheres elongated and coalesced to form PS cylinders. The TEM micrograph of the film obtained from the concentration of $\varphi \sim 13\%$ (v/v) in Figure 2b shows the coexistence of the PS spheres, elongated PS spheres, and PS cylinders. And at the concentration $\varphi \sim 16\%$ (v/v), a predominant in-plane PS cylinder phase appeared. The in-plane and cross-sectional TEM micrographs of such a morphology are shown in Figure 2c. The in-plane view of the film in Figure 2c exhibits PS cylindrical microdomains dispersing in a PMMA matrix. The cross-sectional view of the film in the inset in Figure 2c reveals that the film thickness is ca. 340 nm and that the predominantly in-plane PS cylindrical microdomains disperse in a PMMA matrix and on occasion a cylinder transverses the film, which may correspond to the spherical microdomains which appeared at the in-plane view indicated by the black arrow in Figure 2c. Thus, the phase structure in Figure 2c is inverted cylinders.[13−15]

When the concentration reaches $\varphi \sim 30\%$ (v/v), a locally approximately hexagonal arrangement of "elongated" PMMA "droplets" in a lateral pattern was observed. The TEM micrograph is shown in Figure 2d. Then as the concentration attains $\varphi \sim 40\%$ (v/v), the region of PMMA "droplets" extended to

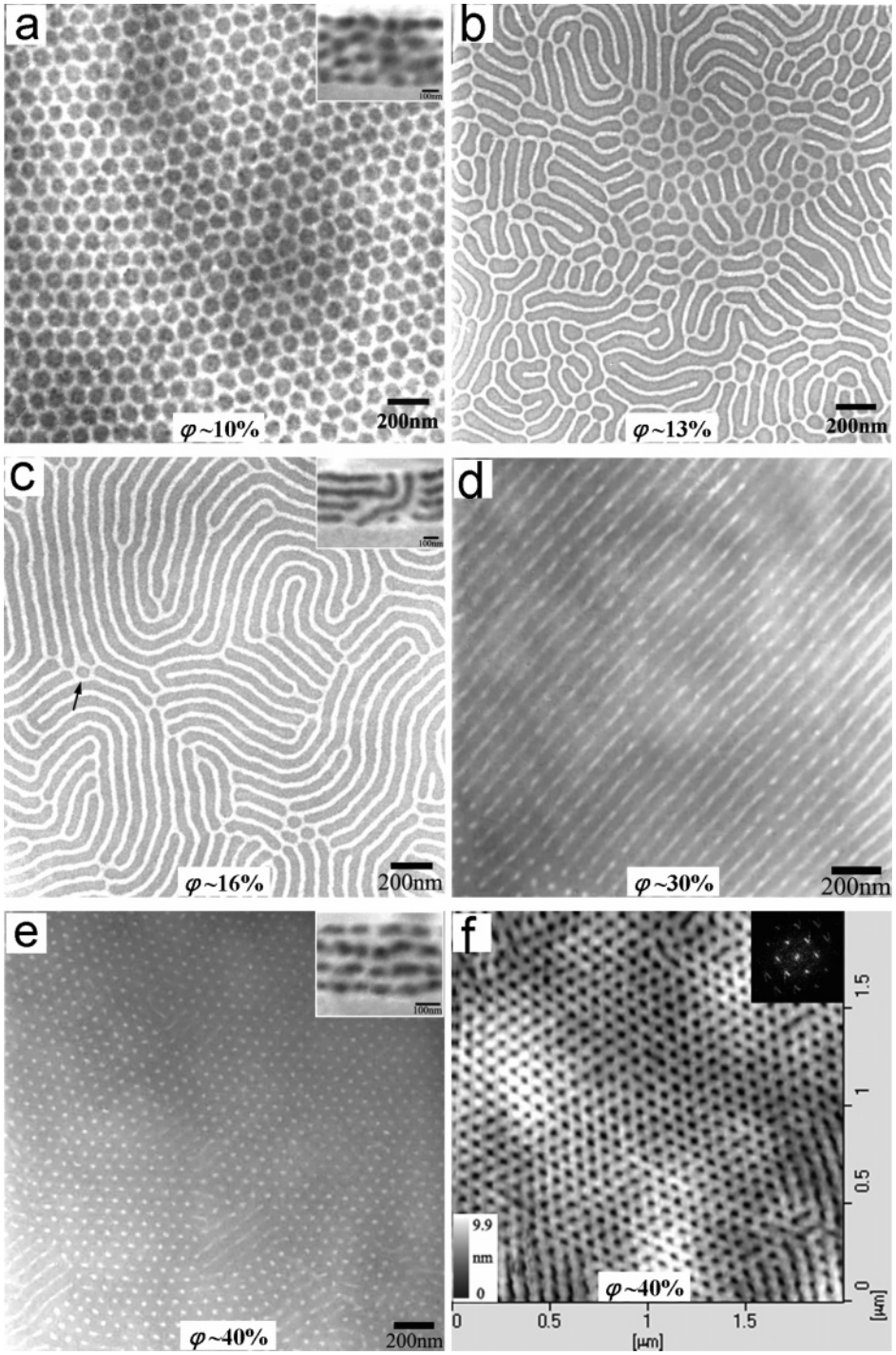

Figure 2. (a−e) Bright-field TEM micrographs of the solution-cast films freeze-dried at different copolymer concentrations as indicated, which show the inverted phase structures. The insets in parts a, c, and e show the cross-sectional TEM micrographs corresponding to their plain view micrographs, respectively. (f) AFM height topography of the film as same as in part e, the right inset shows the two-dimensional fast Fourier transform (2D-FFT) pattern, where the left inset shows the height scale.

the full film. The in-plane and cross-sectional TEM micrographs are shown in Figure 2e, and the AFM height topography is shown in Figure 2f. Combined with the TEM micrograph in Figure 2e, the depressed regions in the AFM height topography in Figure 2f are PMMA. The in-plane pattern in parts e and f of Figure 2 clearly show the PMMA forms the dispersing microdomains, but the cross-sectional TEM micrograph in the inset in Figure 2e shows that the PMMA forms a continuous domain, where the film thickness is ca. 350 nm. This characteristic, together with the two-dimensional fast Fourier transform (2D-FFT) hexagonal pattern obtained from AFM height topography in the inset in Figure 2f, indicates that the morphology observed at $\varphi \sim 40\%$ (v/v) is a hexagonally perforated lamellar (HPL) phase, which has been reported previously for other block copolymers[22,26,32] as well as block/homopolymer blends.[33] An important conclusion from those works is that the occurrence of the HPL phase is bound in composition between the lamellar and cylinder phases at $0.35 \lesssim f \lesssim 0.40$ or $0.63 \lesssim f \lesssim 0.70$, where the minority block forms a layer perforated by the channels of the majority block. Moreover, the same results have been observed by Knoll et al.[20] in block copolymer thin films induced by solvent. Here, we deem that the phase structure

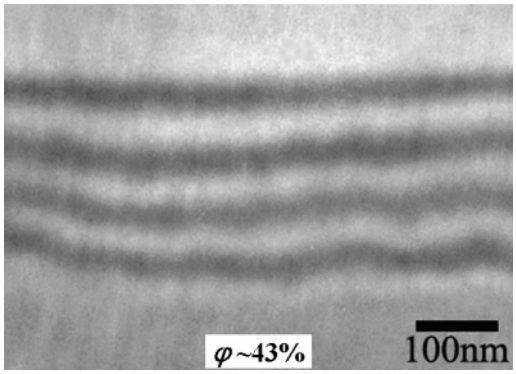

Figure 3. Cross-sectional TEM micrograph of the solution-cast film freeze-dried at $\varphi \sim 43\%$ (v/v), which shows the lamellar phase structure.

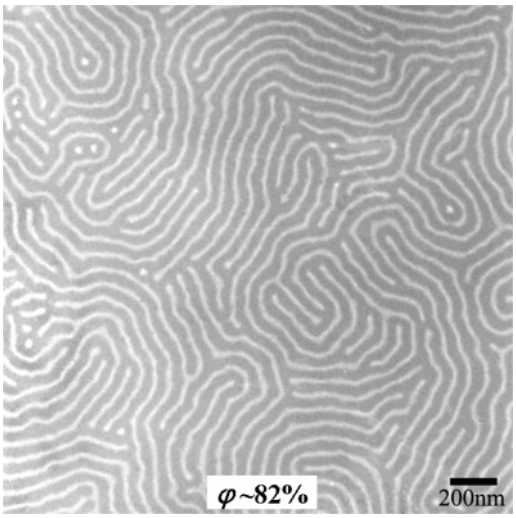

Figure 4. Bright-field TEM micrograph of the solution-cast film obtained at $\varphi \sim 82\%$ (v/v), which shows the normal cylinder phase structure.

shown in parts e and f of Figure 2 should be described as an inverted hexagonally perforated lamellar (IHPL) phase since the perforated layer is composed of the majority PS block (a more detailed explanation will be given in discussion section). Correspondingly, the structure obtained at the concentration $\varphi \sim 30\%$ (v/v) in Figure 2d, as a transitional structure from inverted cylinders (Figure 2c) to inverted hexagonally perforated lamellae (IHPL) (parts e and f of Figure 2), may best be described as an undulated inverted cylinders (UIC) phase, where the surface of the inverted cylinders is undulated possibly due to the solvent content fluctuation.[34,35]

As for the film obtained at $\varphi \sim 43\%$ (v/v), there are no lateral structures on top of the film were detected. This finding, together with the cross-sectional TEM micrograph in Figure 3 in which parallel alternate PS and PMMA stripes exist, indicates that a parallel lamellar phase was obtained. The film thickness is ca. 280 nm. The same lamellar phase structure was also observed in the film obtained from the concentration of $\varphi \sim 55\%$ (v/v).

The copolymer concentration increases rapidly as the amount of solvent further decreases, it is difficult to trap the film structure in detail. Finally, in the case of $\varphi \gtrsim 82\%$ (v/v), an equilibrium structure was consistently observed. Here, we show a typical TEM micrograph of the film obtained at $\varphi \sim 82\%$ (v/v) in Figure 4, in which predominant in-plane PMMA cylinders are dispersed in a PS matrix. The average microdomain spacing is 67 ± 2 nm.

Discussion

For the PS-*b*-PMMA diblock copolymer, the Flory−Huggins interaction parameter, χ, was measured by Russell et al.[36] to be $\chi = 0.028 \pm 0.002 + (3.9 \pm 0.06)/T$. At room temperature ($\sim 25$ °C) the product χN for the block copolymer used in the present work PS_{1257}-*b*-$PMMA_{460}$ is 64, suggesting that the equilibrium phase structure is PMMA cylinders dispersing in a PS matrix.[1] However, with the copolymer concentration increasing, the morphology of the solution-cast film goes through a disordered sphere phase (Figure 1), a series of inverted phases (Figure 2), and a lamellar phase (Figure 3), before it reaches the normal cylinder phase (Figure 4). In contrast to the previous studies that the inverted phase was observed in block copolymers (SBS and SB) including a low modulus PB block,[13−15] the inverted phase observed in this work is from a diblock copolymer in which the two components PS and PMMA have comparable bulk moduli. Therefore, we can rationally deduce that the inverted phase formed in this work is hardly modulus (viscoelasticity) dependent. Moreover, although complex phase behavior of cylinder-forming block copolymers can be obtained by relying on the boundary conditions of a film,[20,25,26] our previous work[16] has confirmed that the boundary effect extends into the bulk of the film with a decay length of about one microdomain spacing, ~ 67 nm for the present block copolymer. The thickness of the film controlled in this work ($\gtrsim 280$ nm) is much higher than one microdomain spacing, and it is therefore reasonable to expect that the phase behavior found in this work is hardly related to the boundary conditions of the film. In contrast, as shown in the insets in parts a, c, and e of Figures 2 and 3, the structure of the solution-cast film is uniform between the surface and the interior, the rich morphological polymorphism of as-cast films having comparable thicknesses which strongly depend on the copolymer concentrations. In the following section, in view of different copolymer solution concentrations, we first explain the disordered sphere phase obtained in low concentration solution and then discuss the inverted to normal phase transition with increasing concentration.

Disordered Spheres Phase. As shown in Figure 1, a disordered micelle-like spheres phase in which the spheres consist of the majority PS block as a core and the minority PMMA block as a corona is detected in as-cast films obtained by freeze-drying the samples at copolymer concentrations $\varphi \sim 0.1\%$ and 1% (v/v). Because the morphologies of the films are trapped by freeze-drying, such morphologies in films are the memory of the phase structures in solutions.[13] In fact, the observation of the majority block aggregates in dilute solution is not surprising in itself, provided the solvent used is selectively good for the minority block.[1,31] However, the solvent (Tetra-CE) used in this work is good for both blocks, although it shows preferential affinity for the minority PMMA block since the difference between the two polymer−solvent interaction parameters ($\Delta\chi = \chi_{PS\text{-}Tetra\text{-}CE} - \chi_{PMMA\text{-}Tetra\text{-}CE}$) is 0.06. According to the mean-field theory, the microphase separation for the present block copolymer/nominal neutral solvent system will take place at $\varphi \sim 16\%$ (v/v),[37−39] so the thermodynamical driving force for the disordered sphere phase formation in such a low concentration solution thereby needs to be considered.

As far as the block copolymers in solution are concerned, the phase behavior in highly dilute solution, where the entropy of the system is expected to play a key role, is an attracting area.[6,40,41] By examining a mutual good solvent (toluene) effect on the conformations of each block of PS-*b*-PMMA diblock copolymer, Tanaka et al.[40] have demonstrated the formation of a certain ordered structure in the concentration region much

lower than the microphase separation concentration predicted by mean-field theory. Meanwhile, they have proposed that the diblock copolymer can be modeled as two Gaussian density bodies of PS and PMMA separated by a certain distance. On the other hand, on the basis of the measurement of the coefficients of the binary interaction terms, the mutual diffusion coefficient, and the second and third virial coefficients, Lodge et al.[41] have pointed out that, at low but finite concentration, a weak ordering effect may exist in PS-*b*-PMMA/toluene solution far from the conditions where microphase separation occurs. Our finding in this work in Figure 1, together with those results, is reminiscent of the colloid aggregation induced by depletion attraction in dilute solutions.[42−45] The depletion attraction was first recognized by Asakura and Oosawa[46] and is considered to have an entirely entropy origin. In a binary mixture of large and small spheres, there is some volume around the large spheres not accessible by the small spheres, which is called excluded volume. If two large spheres are closer to each other than the diameter of the small spheres, the excluded volume overlaps among the large spheres and diminishes the total amount of excluded volume. Consequently, the free volume of the system increases and accordingly the translational entropy increases. That is, the gain in translational entropy of the system due to free volume increase compensates for the loss in mixing entropy resulting from the aggregation.

In the present PS-*b*-PMMA/Tetra-CE copolymer/solvent system, it seems to be a system consisting of "soft colloids"[40,47] and solvent molecules, i.e., "soft colloids" of PS with larger size and "soft colloids" of PMMA with smaller size separated by a certain distance and solvent molecules with a much smaller size. Since solvent molecules display preferential affinity for the smaller size PMMA soft colloids, it seems there are more solvent molecules as PMMA's partner. As a result, the total amount of PMMA soft colloids plus solvent molecules as PMMA's partner is expected to be more than that of the PS soft colloids plus solvent molecules as PS's partner. Moreover, it has been known that depletion attraction is prominent in the system with lower concentration of the larger colloids. Therefore, in dilute solution such as $\varphi \sim 0.1\%$ (v/v), the larger size PS soft colloids easily aggregate to make the block copolymer form micelle-like spheres with a PS core surrounded by a PMMA corona like that in Figure 1 to increase the free volume of the system. Thus, the translational entropy gain due to such increase in the free volume compensates for the mixing entropy reduction due to the aggregation of PS. Here, it should be mentioned that the size of the aggregates, 85 ± 5 nm in diameter as shown in Figure 1, cannot expand infinitely due to the three parameters controlling the geometry of the aggregates, such as the stretching of the core-forming blocks in the core, the repulsive interaction among the corona chains, and the interfacial tension at the core−corona interface.[31]

Inverted to Normal Phase Transition. As the copolymer concentration attains a critical value, the PMMA coronas coalesce to form a continuous matrix and hence a compact morphology is favored. That is, morphology of close-packed PS spheres dispersing in a PMMA matrix as shown in Figure 2a is constructed, which is a typical inverted phase—the minority PMMA block comprising the continuum phase.[13−16]

Although the majority PS in the present block copolymer forming the dispersing microdomains is not thermodynamically favored in the absence of solvent, a block copolymer solution allows the possibility of forming the transient "inverted" phase in which the majority PS block preferentially aggregates as described above due to the solvent having preferential affinity for the minority PMMA block. By rapidly freezing-in the sample in that situation, such a transient phase structure can be trapped in thin films. On the other hand, the difference between the two polymer−solvent interaction parameters ($\Delta\chi = 0.06$) is sufficient to make the stretching degree of the less soluble PS chain lower than that of the more soluble PMMA chain.[40,48] Moreover, the previous study has revealed that the solvent diffusion coefficient in a polymer is strongly dependent on the degree of polymer chain stretching, that is, the higher the degree of polymer chain stretching is, the swifter the solvent diffuses in that domain.[49] In addition, the solvent Tetra-CE is still good for both PS and PMMA blocks and the difference of the solvent distribution between the two domains should be quite small. Therefore, it is reasonable to expect that above a critical copolymer concentration the departure of solvent from the more stretching PMMA domain should be faster than that from the highly entangled PS domain. As a result, with the solvent evaporation, the volume fraction of PMMA plus solvent (the effective volume fraction of PMMA) decreases step by step until its original value, i.e., the bulk volume fraction. We infer that it is such reduction of effective volume fraction of PMMA with the solvent evaporation that dominates the alteration of the interfacial curvature to minimize the free energy of the system[1,50] and to accomplish the transition from inverted spheres (Figure 2a) to normal cylinders (Figure 4), through a series of transient phases (parts b−f of Figures 2 and 3).

According to a theoretical study by Huang and Lodge,[51] the phase transition from inverted to normal phase should be expected as the copolymer concentration increases when a strongly selective solvent for the minority block is used and the difference between two polymer−solvent interaction parameters is as large as 0.2. However, in our previous paper,[13] it has been significantly found that the small degree of preferential affinity like $\Delta\chi = 0.06$ of toluene for the minority PS block can induce the inverted to normal phase transition to occur for both cylinder-forming SBS and SB block copolymers with large differences in the component modulus. In this work, for a very different material which consists of two components with comparable bulk modulus, PS and PMMA, our experimental results in Figures 2−4, indeed, further demonstrate that such a small degree of preferential affinity of Tetra-CE for the minority PMMA block as $\Delta\chi = 0.06$ is enough to make it possible to form the inverted phase and to accomplish the transition from inverted to normal phase with the copolymer concentration increasing. Moreover, a rich phase sequence from inverted to normal phase involving the interface curvature alteration was observed (Figures 2−4).

In addition, it is interesting to note that an unconventional phase structure, the inverted hexagonally perforated lamellar (IHPL) phase as shown in parts e and f of Figure 2 between the inverted cylinder (Figure 2c) and lamellar (Figure 3) phases, was also observed. Although the normal hexagonally perforated lamellar phase in which the layer of minority block is perforated by the channels of the majority block has been discovered in both block copolymer thin films[20,22,26] and bulk,[32] the IHPL phase with the majority PS block forming a layer perforated by the channels of the minority PMMA block as shown in parts e and f of Figure 2 was first detected in this work. On the basis of both surface energy and volume fraction considerations, one may argue that the majority PS block with lower surface energy (40.7 dyn/cm[52]) tends to accumulate at the surface, and hence the morphology of the layer of the minority PMMA block with higher surface energy (41.1 dyn/cm[52]) perforated by the channels of the majority PS block is thermodynamically favored.[20,26]

However, as mentioned above, the IHPL shows that the layer of PS is perforated by the channels of PMMA, which simultaneously appears at the surface as well as in the interior of the film. Here, since the surface energy difference between the two blocks is as small as 0.4 dyn/cm, it is expected to be easily counteracted by the solvent preferential affinity for the PMMA block. Moreover, the fact that the swollen minority PMMA block has already formed the continuum phase makes it difficult for the majority PS block to form a whole layer in that situation. At the same time, with solvent reduction, the effective volume of PMMA decreases and accordingly withdraws from the layer containing PS microdomains to decrease the interfacial energy. During the withdrawing process, the PMMA possibly leaves behind some remnant at that layer and hence forms the perforating channels. Thereby, it is expected that the effective volume fraction of each domain still plays a key role in such IHPL transient phase structure formation.

With the amount of solvent further reducing the effective volume of PMMA has thoroughly withdrawn from the hybrid layer of PS and PMMA microdomains and induced the PS to form a whole layer (Figure 3). Then as the amount of solvent remnant is small enough, the dominant effect of the solvent almost vanishes. Hence, the equilibrium phase−normal cylinder phase in Figure 4 was formed.

Conclusions

The inverted phase formation and the phase transition from inverted to normal of a cylinder-forming PS-*b*-PMMA diblock copolymer in Tetra-CE-solution-cast films with a thickness of about 300 nm during the solution concentrating process by slow solvent evaporation have been studied, where Tetra-CE is a good solvent for both blocks but has preferential affinity for the minority PMMA block. The freeze-drying method enabled us to successfully make observations of the phase structure in solution-cast films at different solvent evaporation times corresponding to the one in solution at different block copolymer concentrations, φ. With the solution becoming more concentrated, the phase sequence of the solution-cast film is disordered spheres (DS), inverted spheres (IS), inverted cylinders (IC), inverted hexagonally perforated lamellae (IHPL), lamellae (LAM), and finally reaches normal cylinders (NC). Such complicated phase behavior was mainly attributed to the solvent nature and the copolymer concentration. Since the solvent exhibits preferential affinity for the minority PMMA block, the depletion attraction might dominate the phase formation in dilute solution, which induces the majority PS block to aggregate to form micelle-like disordered spheres consisting of a core formed by the majority PS block surrounded by a PMMA corona. With the copolymer concentration increasing, the difference in chain conformation between swollen PS and PMMA domains is expected to influence the rate of solvent departure from each domain. It changes the effective volume fractions of each domain and accordingly induces the system to accomplish the interfacial curvature alteration and as a result to drive the inverted phase to transform back to the normal phase. The results obtained in this work, together with our previous study about inverted phase formation for SBS and SB block copolymers,[13] suggest that the inverted phase formation and the transition from inverted to normal phase with the copolymer concentration increasing might be a universal feature of cylinder-forming block copolymer films cast from a good solvent with a preferential affinity for the minority block.

Acknowledgment. We are grateful to Prof. C. Wu at the Chinese University of Hong Kong and Prof. S. Bo at Changchun Institute of Applied Chemistry for helpful discussions. This work was supported by the National Science Foundation of China (20574068) and the Chinese Academy of Sciences (KJCX2-SW-H07) and subsidized by the National Basic Research Program of China (2005CB6238).

Supporting Information Available: Plot of the average calculated copolymer concentration in the solution-cast film vs solvent evaporation time. This material is available free of charge via the Internet at http://pubs.acs.org.

References and Notes

(1) Hamley, I. W. *The Physics of Block Copolymers*; Oxford University Press: New York, 1998.
(2) Fasolka, M. J.; Mayes, A. M. *Annu. Rev. Mater. Res.* **2001**, *31*, 323.
(3) Morkved, T. L.; Lu, M.; Urbas, A. M.; Ehrichs, E. E.; Jaeger, H. M.; Russell, T. P. *Science* **1996**, *273*, 931.
(4) Thurn-Albrecht, DeRouchey, J.; Russell, T. P.; Jaeger, H. M. *Macromolecules* **2000**, *33*, 3250.
(5) Henkee, C. S.; Thomas, E. L.; Fetters, L. J. *J. Mater. Sci.* **1988**, *23*, 1685.
(6) Buck, E.; Fuhrmann, J. *Macromolecules* **2001**, *34*, 2172.
(7) Fukunaga, K.; Elbs, H.; Magerle, R.; Krausch, G. *Macromolecules* **2000**, *33*, 947.
(8) Elbs, H.; Drummer, C.; Abetz, V.; Krausch, G. *Macromolecules* **2002**, *35*, 5570.
(9) Chen, Y.; Huang, H.; Hu, Z.; He, T. *Langmuir* **2004**, *20*, 3805.
(10) Funaki, Y,; Kumano, K.; Nakao, T.; Jinnai, H.; Yoshida, H.; Kimishima, K.; Tsutsumi, K.; Hirokawa, Y.; Hashimoto, T. *Polymer* **1999**, *40*, 7147.
(11) Kim, J.; Kim, B.; Jung, B.; Kang, Y. S.; Ha, H. Y.; Oh, I.-H.; Ihh, K. J. *Macromol. Rapid Commun.* **2002**, *23*, 753.
(12) Cong, Y.; Li, B.; Han, Y.; Li, Y.; Pan, C. *Macromolecules* **2005**, *38*, 9836.
(13) Huang, H.; Hu, Z.; Chen, Y.; Zhang, F.; Gong, Y.; He, T.; Wu, C. *Macromolecules* **2004**, *37*, 6523.
(14) Huang, H.; Zhang, F.; Hu, Z.; Du, B.; He, T.; Lee, F. K.; Wang, Y.; Tsui, O. K. C. *Macromolecules* **2003**, *36*, 4084.
(15) Zhang, Q.; Tsui, O. K. C.; Du, B.; Zhang, F.; Tang, T.; He, T. *Macromolecules* **2000**, *33*, 9561.
(16) Gong, Y.; Hu, Z.; Chen, Y.; Huang, H.; He, T. *Langmuir* **2005**, *21*, 11870.
(17) Kim, S. H.; Misner, M. J.; Xu, T.; Kimura, M.; Russell, T. P. *Adv. Mater.* **2004**, *16*, 226.
(18) Kim, G.; Libera, M.*Macromolecules* **1998**, *31*, 2569.
(19) Niu, S.; Saraf, R. F. *Macromolecules* **2003**, *36*, 2428.
(20) Knoll, A.; Horvat, A.; Lyakhova, K. S.; Krausch, G.; Sevink, G. J. A.; Zvelindovsky, A. V.; Magerle, R. *Phys. Rev. Lett.* **2002**, *89*, 035501. Knoll, A.; Magerle, R.; Krausch, G. *J. Chem. Phys.* **2004**, *120*, 1105.
(21) Russell, T. P.; Coulon, G.; Deline, V. R.; Miller, D. C. *Macromolecules* **1989**, *22*, 4600.
(22) Fasolka, M. J.; Banerjee, P.; Mayes, A. M.; Pickett, G.; Balazs, A. C. *Macromolecules* **2000**, *33*, 5702.
(23) Huang, E.; Rockford, L.; Russell, T. P.; Hawer, C. J.; Mays, J. *Nature* **1998**, *395*, 757.
(24) Fukunaga, K.; Hashimoto, T.; Elbs, H.; Magerle, R.; Krausch, G. *Macromolecules* **2002**, *35*, 4406.
(25) Böker, A.; Müller, A. H. E.; Krausch, G. *Macromolecules* **2001**, *34*, 7477.
(26) Radzilowski, L. H.; Carvalho, B. L.; Thomas, E. L. *J. Polym. Sci., Part B: Polym. Phys.* **1996**, *34*, 3081.
(27) *Polymer Handbook*, 3rd ed.; Brandrup, J.; Immergut, E. H., Eds.; John Wiley & Sons: New York, 1989.
(28) Huo, Y.; Zhang, H.; Yang, Y. *Macromolecules* **2003**, *36*, 5383.
(29) *Properties of Polymers*; Van Krevelen, D. W., Ed.; Elsevier Scientific Publishing Company: Amsterdam, Oxford, U.K., and New York, 1976.
(30) Cantor, A. S.; Pecora, R. *Macromolecules* **1994**, *27*, 6812.
(31) Zhang, L.; Eisenberg, A. *J. Am. Chem. Soc.* **1996**, *118*, 3168.
(32) Almdal, K.; Koppi, K. A.; Bates, F. S.; Mortensen, K. *Macromolecules* **1992**, *25*, 1743. Hamley, I. W.; Koppi, K. A.; Rosedale, J. H.; Bates, F. S.; Almdal, K.; Mortensen, K. *Macromolecules* **1993**, *26*, 5959. Förster, S.; Khandpur, A. K.; Zhao, J.; Bates, F. S.; Hamley, I. W.; Ryan, A. J.; Bras, W. *Macromolecules* **1994**, *27*, 6922. Khandpur, A. K.; Förster, S.; Bates, F. S.; Hamley, I. W.; Ryan, A. J.; Bras, W.; Almdal, K.; Mortensen, K. *Macromolecules* **1995**, *28*, 8796. Schulz,

M. F.; Khandpur, A. K.; Bates, F. S.; Almdal, K.; Mortensen, K.; Hajduk, D. A.; Gruner, S. M. *Macromolecules* **1996**, *29*, 2857.
(33) Spontak, R. J.; Smith, S. D.; Ashraf, A. *Macromolecules* **1993**, *26*, 956. Disko, M. M.; Liang, K. S.; Behal, S. K.; Roe, R. J.; Jeon, K. J. *Macromolecules* **1993**, *26*, 2983.
(34) Ryu, C. Y.; Vigild, M. E.; Lodge, T. P. *Phys. Rev. Lett.* **1998**, *81*, 5354.
(35) Laradji, M.; Shi, A.-C.; Desai, R. C.; Noolandi, J. *Phys. Rev. Lett.* **1997**, *78*, 2577.
(36) Russell, T. P.; Hjelm, R. P.; Seeger, P. A. *Macromolecules* **1990**, *23*, 890.
(37) Fredrickson, G. H.; Leibler, L. *Macromolecules* **1989**, *22*, 1238.
(38) Helfand, E.; Tagami, Y. *J. Chem. Phys.* **1972**, *56*, 3592.
(39) Whitmore, M. D.; Vavasour, J. D. *Macromolecules* **1992**, *25*, 2041. **1992**, *25*, 5477. **1993**, *26*, 7070.
(40) Tanaka, T.; Kotaka, T.; Inagaki, H. *Macromolecules* **1974**, *7*, 311. **1976**, *9*, 561.
(41) Kent, M. S.; Tirrell, M.; Lodge, T. P. *J. Polym. Sci., Part B: Polym. Phys.* **1994**, *32*, 1927.
(42) Lekkerkerker, H. N. W.; Stroobants, A. *Nature (London)* **1998**, *393*, 305.
(43) Adams, M.; Dogic, Z.; Keller, S. L.; Fraden, S. *Nature (London)* **1998**, *393*, 349.
(44) Daoud, M.; Williams, C. E. *Softer Matter Physics*; Springer-Verlag: Berlin and Heidelberg, Germany, 1999.
(45) Helden, L.; Roth, R.; Koenderink, G. H.; Leiderer, P.; Bechinger, C. *Phys. Rev. Lett.* **2003**, *90*, 048301. Helden, L.; Roth, R.; Koenderink, G. H.; Leiderer, P.; Bechinger, C. *Langmuir* **2004**, *20*, 5662.
(46) Asakura, S.; Oosawa, F. *J. Chem. Phys.* **1954**, *22*, 1255. Asakura, S.; Oosawa, F. *J. Polym. Sci.* **1958**, *33*, 183.
(47) Louis, A. A.; Bolhuis, P. G.; Hansen, J. P.; Meijer, E. J. *Phys. Rev. Lett.* **2000**, *85*, 2522.
(48) Han, C. C.; Mozer, B. *Macromolecules* **1974**, *7*, 44.
(49) Jonquières, A.; Clément, R.; Lochon, P. *Prog. Polym. Sci.* **2002**, *27*, 1803.
(50) Lodge, T. P.; Xu, X.; Ryu, C. Y.; Hamley, I. W.; Fairclough, J. P. A.; Ryan, A. J.; Pedersen, J. S. *Macromolecules* **1996**, *29*, 5955.
(51) Huang, C.-I.; Lodge, T. P. *Macromolecules* **1998**, *31*, 3556.
(52) Green, P. F.; Christensen, T. M.; Russell, T. P.; Jérôme, R. *Macromolecules* **1989**, *22*, 2189.

MA052380K